POLITECNICO DI TORINO
Repository ISTITUZIONALE

Rh/CeO2 thin catalytic layer deposition on alumina foams: Catalytic performance and controlling regimes in biogas reforming processes

Original
Rh/CeO2 thin catalytic layer deposition on alumina foams: Catalytic performance and controlling regimes in biogas reforming processes / Italiano, C.; Ashraf, M. A.; Pino, L.; Moncada Quintero, C. W.; Specchia, S.; Vita, A.. - In: CATALYSTS. - ISSN 2073-4344. - ELETTRONICO. - 8:448(2018), pp. 1-24. [10.3390/catal8100448]

Availability:
This version is available at: 11583/2715036 since: 2018-10-12T14:58:10Z

Publisher:
MDPI

Published
DOI:10.3390/catal8100448

Terms of use:
openAccess

This article is made available under terms and conditions as specified in the corresponding bibliographic description in the repository

Publisher copyright

(Article begins on next page)

30 September 2022

Supplementary Materials: Rh/CeO_2 thin catalytic layer deposition on alumina foams: catalytic performance and controlling regimes in biogas reforming processes

Cristina Italiano *, Muhammad Arsalan Ashraf, Lidia Pino, Carmen Williana Moncada Quintero, Stefania Specchia and Antonio Vita

S.1. SEM images

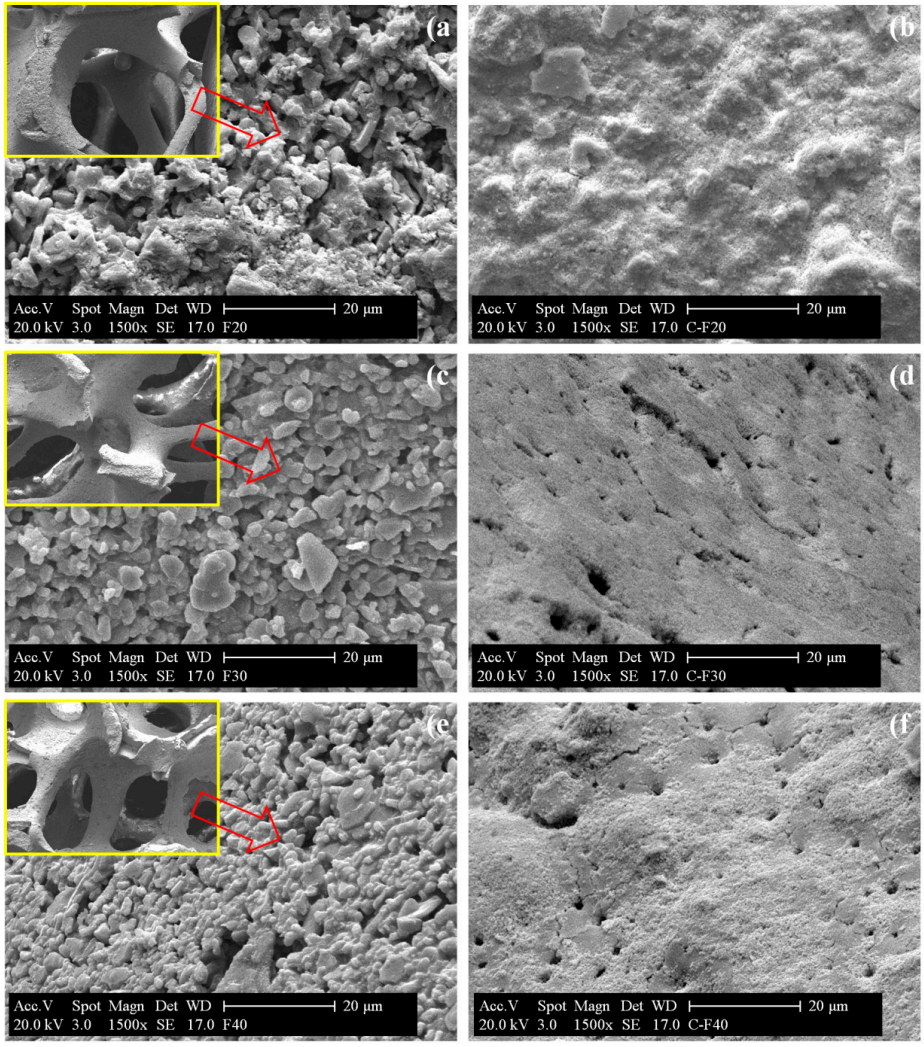

Figure S1. SEM micrographs of bare (**a**, **c**, **e**) and Rh/CeO_2-coated (**b**, **d**, **f**) OCFs: F20 (**a**, **b**), F30 (**c**, **d**) and F40 (**e**, **f**) structures (inset: images of the macroscopic bare OFCs).

An irregular porous surface was evidenced in SEM images of bare OCFs (Figure S.1 a, c, e) while a reduction of the macro-porosity of the alumina surface was revealed after depositing the catalytic layer (Figure S1b, d, f).

S.2. XRD measurements

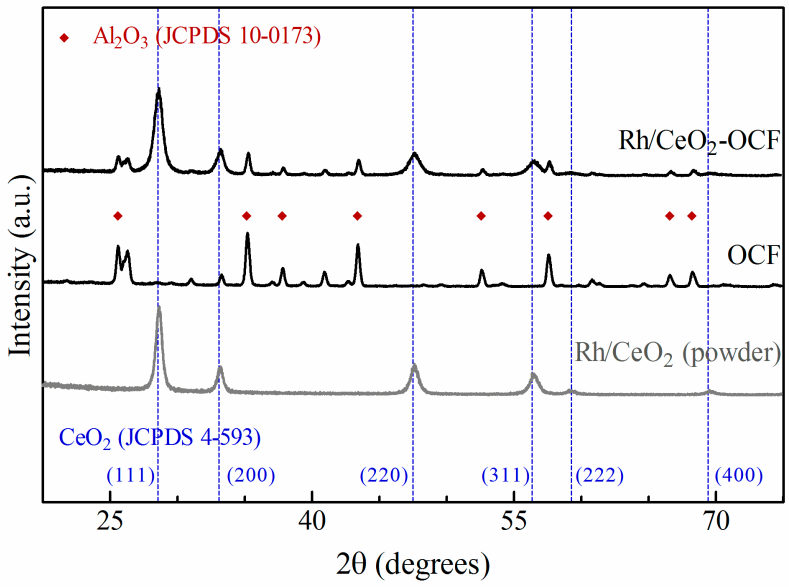

Figure S2. XRD pattern of Rh/CeO_2 as a powder, bare and Rh/CeO_2-coated F30 (included also reference peaks of CeO_2: JPDS 4-593 and reference peaks of Al_2O_3: JPDS 10-0173).

Figure S2 shows X-ray diffraction patterns of bare and Rh/CeO_2-coated 30 ppi OCF, and Rh/CeO_2 in powder form. In the Rh/CeO_2 powder, the diffraction peaks can be assigned to the crystal planes of face-centered cubic CeO_2 (JCPDS 4-593) with typical diffraction peaks at 28.55° (111), 33.08° (200), 47.50° (220), 56.33° (311), 59.26° (222), and 69.41° (400) [1]. No diffraction peaks of Rh oxides were detected, due to the low loading and high dispersion of the noble metal [2]. The analysis of the diffraction pattern of bare 30 ppi OCF allowed the identification of α-Al_2O_3 phase (JCPDS 10-0173), with peaks located at 25.59° (012), 35.16° (104) 37.81° (110), 43.38° (113) 52.58° (024), 57.52° (116), 66.57° (214) and 68.27° (306) [3,4]. As expected, both cubic CeO_2 fluorite type and α-Al_2O_3 phase were identified after depositing the Rh/CeO_2 catalytic layer on the 30 ppi OCF [5]. The average crystallite size, calculated by the Scherrer equation from the main CeO_2 (111) reflection, was found to be 14.8 nm for Rh/CeO_2 powder catalyst and 11.2 nm for Rh/CeO_2 deposited on the foam. Almost equal results (not shown) were obtained for F20 and F40 structured catalysts.

S.3. Mass and heat transport limitations

In the following, a detailed explanation of fluid properties determination, characteristic time analysis and dimensionless numbers calculation is provided.

Gas, gas-solid and solid properties

Molecular weight (M_{mix}), density (ρ_{mix}) and, viscosity (μ_{mix}) of gas mixture were calculated as:

$$M_{mix} = \sum_{i=1}^{n} y_i \, M_i \tag{S1}$$

$$\rho_{mix} = \frac{P \, M_{mix}}{R \, T} \tag{S2}$$

$$\mu_{mix} = \frac{\sum_{i=1}^{n} \mu_i \, y_i \, M_i^{1/2}}{\sum_{i=1}^{n} y_i \, M_i^{1/2}} \tag{S3}$$

where gas viscosity of a single component (μ_i) was calculated from a corresponding state method [6].

For CH_4, CO_2, CO, and N_2 it was calculated by Equation S4, using the tabulated values of $T_{c,i}$ and $P_{c,i}$ [7].

$$\mu_i = \frac{64.008 \cdot 10^{-5} \left(4.5 \frac{T}{T_{c,i}} - 1.67\right)^{0.625}}{0.176\, T_{c,i}^{1/6}\, M_i^{-1/2}\, P_{c,i}^{-2/3}} \quad \text{(S4)}$$

	CH_4	CO_2	CO	N_2
$T_{c,i}$ **(K)**	190.7	304.1	133.0	126.2
$P_{c,i}$ **(kPa)**	46.4	73.7	35.0	33.9

For H_2 and H_2O it was calculated by Equations S5 and S6, respectively.

$$\mu_{H_2} = 326.55 \cdot 10^{-5} \,(0.1375\, T - 1.167)^{0.625} \quad \text{(S5)}$$

$$\mu_{H_2O} = 1170.828 \cdot 10^{-5} \,(0.011662\, T - 0.551) \quad \text{(S6)}$$

Diffusivity of CH_4 in gas phase (D_{CH_4}) was calculated from the binary diffusion of CH_4 and i gas species (D_{CH_4-i}) by:

$$D_{CH_4} = \frac{1 - y_{CH_4}}{\sum_{i=1;i\neq CH_4}^{n} \frac{y_i}{D_{CH_4-i}}} \quad \text{(S7)}$$

where D_{CH_4-i} was determined by Fuller equation (Equation S8) [8], using tabulated values of v_i [7].

$$D_{CH_4-i} = \frac{10^{-3}\, T^{1.75} \left(\frac{1}{M_{CH_4}} + \frac{1}{M_i}\right)^{1/2}}{\frac{P}{101.325}\left(v_{CH_4}^{1/3} + v_i^{1/3}\right)^2} \quad \text{(S8)}$$

	CH_4	CO_2	CO	N_2	H_2	H_2O
v_i **(cm³·mol⁻¹)**	24.4	26.9	18.9	17.9	7.1	12.7

Mass transfer coefficient of CH_4 (k_G) was determined from the Sherwood number (*Sh*) by:

$$k_G = \frac{Sh\, D_{CH_4}}{d_{p,c}} \quad \text{(S9)}$$

Sh was calculated from Reynold (*Re*) and Schmidt (*Sc*) numbers by Equations S10, S11 and S12 [9–12].

$$Sh = 1.00\, Re^{0.47}\, Sc^{0.33} \left(\frac{d_{f,c}}{0.001m}\right)^{0.58} \varepsilon^{0.44} \quad \text{(S10)}$$

$$Re = \frac{d_{p,c}\, u\, \rho_{mix}}{\mu_{mix}} \quad \text{(S11)}$$

$$Sc = \frac{\mu_{mix}}{\rho_{mix}\, D_{CH_4}} \quad \text{(S12)}$$

where the average coated face diameter ($d_{f,c}$) and the average coated pore diameter ($d_{p,c}$) were determined according to Equations S13 and S14, respectively:

$$d_{f,c} = d_f + 2\,\delta_c \tag{S13}$$

$$d_{p,c} = d_p - 2\,\delta_c \tag{S14}$$

while the inlet gas velocity (u) at standard temperature (T_S) and pressure (P_S) was calculated from Equation S15:

$$u = \frac{F_{tot}}{OFA\;\varepsilon}\,\frac{T}{T_S}\,\frac{P}{P_S} \quad \text{with} \quad OFA = \frac{\pi\,\phi^2}{4} \tag{S15}$$

Effective diffusivity of CH_4 in coated layer ($D_{CH_4,e}$) was calculated from the Knudsen diffusion (D_k) by the Equation [13–15]:

$$D_{CH_4,e} = \frac{\varepsilon_c}{\tau}\left(\frac{1}{D_{CH_4}} + \frac{1}{D_k}\right)^{-1} \tag{S16}$$

where ε_c is the coated layer porosity ($\varepsilon_c = \rho_c\,PV_{BJH} = 0.12$) [16], τ is the tortuosity factor ($\tau = 1 - ln\varepsilon_c = 3.12$) [17] and D_k was determined by equation S17 [18]:

$$D_k = 9.7 \cdot 10^{-5}\,r_p\left(\frac{T}{M_{CH_4}}\right)^{-1/2} \tag{S17}$$

Average values of specific surface area ($SA_{BET} = 24$ $m^2 \cdot g^{-1}$) and pore volume ($PV_{BJH} = 0.06$ $cm^3 \cdot g^{-1}$) were determined from Brunauer-Emmett-Teller (BET) and Barrett-Joyner-Halenda (BJH) analytic methods for N_2 adsorption-desorption isotherms of the structured catalysts. Pore radius ($r_p = 50$ Å) was given by $2PV_{BJH}/SA_{BET}$ equation.

The thermal conductivity of the gas mixture (λ_{mix}) was calculated by [19]:

$$\lambda_{mix} = \sum_{i=1}^{n}\frac{y_i\,\lambda_i}{\sum_{j=1}^{n} y_j\,\Phi_{ij}} \quad \text{with} \quad \Phi_{ij} = \frac{1}{\sqrt{8}}\left(1 + \frac{M_i}{M_j}\right)^{-1/2}\left[1 + \left(\frac{\mu_i}{\mu_j}\right)^{1/2}\left(\frac{M_j}{M_i}\right)^{1/4}\right]^2 \tag{S18}$$

where the thermal conductivity of a single gas component (λ_i) was found from the correlation $\lambda_i = A + B \cdot T + C \cdot T^2 + D \cdot T^3$, using tabulated values of *A*, *B*, *C* and *D* constants.

	A	***B***	***C***	***D***
CH₄	−1.869·10⁻³	8.727·10⁻⁵	1.179·10⁻⁷	−3.614·10⁻¹¹
H₂	8.099·10⁻³	6.689·10⁻⁴	−4.158·10⁻⁷	1.562·10⁻¹⁰
H₂O	7.341·10⁻³	-1.013·10⁻⁵	1.801·10⁻⁷	−9.100·10⁻¹¹
N₂	3.919·10⁻⁴	9.816·10⁻⁵	−5.067·10⁻⁸	1.504·10⁻¹¹
CO	5.0678·10⁻⁴	9.125·10⁻⁵	−3.524·10⁻⁸	8.199·10⁻¹²
CO₂	−7.215·10⁻³	8.015·10⁻⁵	5.477·10⁻⁹	−1.053·10⁻¹¹

The gas-solid heat transfer coefficient (h) was calculated from Nusselt number (Nu) by the equation [20]:

$$Nu = \frac{h\,d_{p,c}}{\lambda_{mix}} \tag{S19}$$

where Nu was determined by Equation S20 [21]:

$$Nu = 2.49 \cdot 10^{-8}\, \varepsilon\, T_b + 12.6\, Re \text{ with } T_b = \frac{T_{IN} + T_{OUT}}{2} \quad \text{(S20)}$$

The temperatures registered at the inlet (T_{IN}) and outlet (T_{OUT}) of the catalytic bed during SR and OSR experiments are summarized below. However, experimental errors due to the positioning of thermocouples cannot be excluded.

	WHSV·10³	**SR tests at T=900 °C**		**SR tests at T=800 °C**		**OSR tests at T=900 °C**		**OSR tests at T=800 °C**	
	(Nml g⁻¹·h⁻¹)	T_{IN} **(°C)**	T_{OUT} **(°C)**	T_{IN} **(°C)**	T_{OUT} **(°C)**	T_{IN} **(°C)**	T_{OUT} **(°C)**	T_{IN} **(°C)**	T_{OUT} **(°C)**
20 ppi	34.8	882	912	788	812	910	921	805	820
	69.5	883	922	795	821	915	927	804	822
	139.1	902	925	800	829	900	940	828	820
30 ppi	34.8	895	917	801	821	932	948	857	840
	69.5	897	924	809	827	926	931	831	833
	139.1	906	934	822	834	892	922	801	823
40 ppi	34.8	906	927	827	809	923	931	830	832
	69.5	914	941	829	843	925	939	831	840
	139.1	915	955	828	850	925	942	834	845

Absence of external interphase (gas-solid) heat transfer limitations.

Mears criterion [22] was applied to determine the effect of external interphase (gas-solid) heat transfer limitations by Equation S21:

$$\frac{E_a\, (-\Delta H_r^0)\, R_{CH_4}}{h\, GSA\, R\, T_b^2} < 0.15 \quad \text{(S21)}$$

where E_a and ΔH_r^0 are the apparent activation energy (92 kJ·mol⁻¹) and the standard reaction enthalpy (206.2 kJ·mol⁻¹) [23,24], R_{CH_4} is the observed reaction rate for CH_4 based on foam volume, h is the gas-solid heat transfer coefficient, GSA is the geometric surface area of the OCF, R is the universal gas constant (8.314 J·mol⁻¹ K⁻¹), and T_b is the bulk fluid temperature estimated as in the Equation S20.

Absence of internal heat transfer limitations

Anderson criterion [22,25] was applied to determine the effect of internal heat transfer limitations by Equation S22:

$$\frac{E_a\, (-\Delta H_r^0)\, r_{CH_4}\, \rho_c\, \delta_c^2}{\lambda_c\, R\, T^2} < 0.75 \quad \text{(S22)}$$

where r_{CH_4} is the observed reaction rate for CH_4, ρ_c is the coated layer density, δ_c is the coated layer thickness, λ_c is the effective thermal conductivity of porous materials (assumed equal to 0.3 W·m⁻¹·K⁻¹) [9,20], and T is the reaction temperature.

Characteristic time analysis

The characteristic contact time, or residence time (t_c) describes the flow time of reactants through the OCFs catalysts at feed inlet conditions [26,27]. It was determined by:

$$t_c = \frac{L}{u} \quad \text{(S23)}$$

where L is the OCF length and u is the inlet gas velocity.

The characteristic external mass transfer time (t_{ext}) involves the diffusion of methane from bulk gas to the catalyst surface [28,29]. It was determined by:

$$t_{ext} = \frac{d_{p,c}^2}{4\, D_{CH_4}\, Sh} \tag{S24}$$

where $d_{p,c}$ is the average coated pore diameter, D_{CH_4} is the diffusivity of CH_4 in gas phase and *Sh* is the Sherwood number.

The characteristic coated layer diffusion time (t_{int}) involves the transport of reactants inside the pores of the catalytic layer [30]. It was determined by:

$$t_{int} = \frac{\delta_c^2}{D_{CH_{4,e}}} \tag{S25}$$

where δ_c is the coated layer thickness and $D_{CH_{4,e}}$ is the effective diffusivity of CH_4 in the coated layer.

The characteristic reaction time (t_r) describes the rate of methane conversion [31–33]. It was determined by:

$$t_r = \frac{C_{CH_4}}{r_{CH_4}\, \rho_c} \tag{S26}$$

where C_{CH_4} is the concentration of CH_4 in the feed mixture, r_{CH_4} is the observed reaction rate for CH_4 and ρ_c is the density (2 g·cm^{-3}) of the catalytic layer.

Absence of external and internal mass transfer limitations

Damköhler numbers were determined to describe the trade-off between reaction kinetic and diffusion limitations by Equations S27 (first Damkohler number, *Da-I*), S28 (second Damkohler number, *Da-II*), and S29 (third Damkohler number, *Da-III*) [34–38].

$$Da\text{-}I = \frac{t_c}{t_r} > 1 \tag{S27}$$

$$Da\text{-}II = \frac{t_{ext}}{t_r} < 0.1 \tag{S28}$$

$$Da\text{-}III = \frac{t_{int}}{t_r} < 1 \tag{S29}$$

Carberry [39,40] and Weisz-Prater [30,41,42] numbers were calculated to determine the effect of external and/or internal mass transfer limitation by Equations S30 and S31, respectively.

$$Ca = \frac{R_{CH_4}}{k_G\, GSA\, C_{CH_4}} < 0.05 \tag{S30}$$

$$WP = \frac{r_{CH_4}\, \rho_c\, {\delta_c}^2}{D_{CH_{4,e}}\, C_{CH_{4,s}}} < 1 \tag{S31}$$

where R_{CH_4} is the observed reaction rate for CH_4 based on foam volume and $C_{CH_{4,s}}$ is the concentration of CH_4 at catalyst surface, assumed equal to CH_4 concentration in the feed mixture (C_{CH_4}) in absence of external diffusion controlling regime, otherwise calculated by Equation S32:

$$C_{CH_4,s} = C_{CH_4}(1 - Ca) \quad \text{(S32)}$$

References

1. Italiano, C.; Vita, A.; Fabiano, C.; Laganà, M.; Pino, L. Bio-hydrogen production by oxidative steam reforming of biogas over nanocrystalline Ni/CeO_2 catalysts. *Int. J. Hydrogen Energy* **2015**, *40*, 11823–11830.
2. Palma, V.; Pisano, D.; Martino, M.; Ciambelli, P. Structured catalysts with high thermoconductive properties for the intensification of water gas shift process. *Chem. Eng. J.* **2016**, *304*, 544–551.
3. Zhang, M.; Ning, T.; Sun, P.; Yan, Y.; Zhang, D.; Li, Z. Effect of Al_2O_3-SiO_2 substrate on gas-sensing properties of TiO2 based lambda sensor at high temperature. *Ceram. Int.* **2018**, *44*, 3000–3004.
4. Shi, R.; Shang, Y.; Zhang, Y.; Wang, P.; Zhang, A.; Yang, P. Synthesis of ultrafine α-Al_2O_3 powder by two-step hydrolysis. *Ceram. Int.* **2018**, *44*, 3741–3750.
5. Gómez, L.E.; Tiscornia, I.S.; Boix, A.V.; Miró, E.E. Co preferential oxidation on cordierite monoliths coated with CO/CeO_2 catalysts. *Int. J. Hydrogen Energy* **2012**, *37*, 14812–14819.
6. Bahadori, A. *Natural gas processing: Technology and engineering design*, 1st ed.; Gulf Professional Publishing: Waltham, MA, USA, 2014; pp. 23-58; ISBN 978-0-08-099971-5.
7. Perry, R.H.; Green, D.W.; Maloney, J.O. *Perry's chemical engineers' handbook*, 7th ed.; McGraw-Hill: New York City, NY, USA, 1999; ISBN 0-07-049841-5.
8. Fuller, E.N.; Schettler, P.D.; Giddings, J.C. New method for prediction of binary gas-phase diffusion coefficients. *Ind. Eng. Chem.* **1966**, *58*, 18–27.
9. Ertl, G.; Knözinger, H.; Schüth, F.; Weitkamp, J. Handbook of heterogeneous catalysis, 2nd ed.; Wiley-VCH: Weinheim, Germany, 2008; ISBN 978-3-527-31241-2.
10. Incera Garrido, G.; Patcas, F.C.; Lang, S.; Kraushaar-Czarnetzki, B. Mass transfer and pressure drop in ceramic foams: A description for different pore sizes and porosities. *Chem. Eng. Sci.* **2008**, *63*, 5202–5217.
11. Lucci, F.; Della Torre, A.; von Rickenbach, J.; Montenegro, G.; Poulikakos, D.; Dimopoulos Eggenschwiler, P. Performance of randomized kelvin cell structures as catalytic substrates: Mass-transfer based analysis. *Chem. Eng. Sci.* **2014**, *112*, 143–151.
12. Shah, R.K. Laminar flow friction and forced convection heat transfer in ducts of arbitrary geometry. *Int. J. Heat Mass Transf.* **1975**, *18*, 849–862.
13. von Rickenbach, J.; Lucci, F.; Narayanan, C.; Eggenschwiler, P.D.; Poulikakos, D. Effect of washcoat diffusion resistance in foam based catalytic reactors. *Chem. Eng. J.* **2015**, 276, 388–397.
14. Cao, C.; Zhang, N.; Cheng, Y. Numerical analysis on steam methane reforming in a plate microchannel reactor: Effect of washcoat properties. *Int. J. Hydrog. Energy* **2016**, *41*, 18921–18941.
15. Hayes, R.E.; Kolaczkowskib, S.T.; Li, P.K.C.; Awdry, S. Evaluating the effective diffusivity of methane in the washcoat of a honeycomb monolith. *Appl. Catal. B: Environ.* **2000**, *25*, 93–104.
16. Talebian-Kiakalaieh, A.; Amin, N.A.S. Theoretical and experimental evaluation of mass transfer limitation in gas phase dehydration of glycerol to acrolein over supported HSiW catalyst. *J. Taiwan Inst. Chem. Eng.* **2016**, *59*, 11–17.
17. Kolitcheff, S.; Jolimaitre, E.; Hugon, A.; Verstraete, J.; Carrette, P.-L.; Tayakout-Fayolle, M. Tortuosity of mesoporous alumina catalyst supports: Influence of the pore network organization. *Microporous Mesoporous Mater.* **2017**, *248*, 91–98.
18. Satterfield, C.N. *Mass transfer in heterogeneous catalysis*; MIT Press: Cambridge, MA, USA, 1970; ISBN 0-26-219062-1.
19. Demirel, Y. *Nonequilibrium thermodynamics: Transport and rate processes in physical, chemical and biological systems*, 3rd ed; Elsevier: Amsterdam, 2014; ISBN 978-0-444-59557-7.
20. Fratalocchi, L.; Visconti, C.G.; Groppi, G.; Lietti, L.; Tronconi, E. Intensifying heat transfer in Fischer-Tropsch tubular reactors through the adoption of conductive packed foams. *Chem. Eng. J.* **2018**, 349, 829–837.
21. Richardson, J..; Remue, D.; Hung, J.-K. Properties of ceramic foam catalyst supports: mass and heat transfer. *Appl. Catal. A Gen.* **2003**, *250*, 319–329.

22. Mears, D.E. Diagnostic criteria for heat transport limitations in fixed bed reactors. *J. Catal.* **1971**, *20*, 127–131.
23. Halabi, M.H.; de Croon, M.H.J.M.; van der Schaaf, J.; Cobden, P.D.; Schouten, J.C. Intrinsic kinetics of low temperature catalytic methane–steam reforming and water–gas shift over Rh/$Ce_{\alpha}Zr_{1-\alpha}O_2$ catalyst. *Appl. Catal. A Gen.* **2010**, *389*, 80–91.
24. Hennings, U.; Reimert, R. Stability of rhodium catalysts supported on gadolinium doped ceria under steam reforming conditions. *Appl. Catal. A Gen.* **2008**, *337*, 1–9.
25. Anderson, J.B. A criterion for isothermal behaviour of a catalyst pellet. *Chem Eng. Sci.* **1963**, *18, 147–148*.
26. Laguna, O.H.; Domínguez, M.I.; Centeno, M.A.; Odriozola, J.A. Catalysts on metallic surfaces: Monoliths and microreactors. In *New Materials for Catalytic Applications*; Parvulescu, V.I., Kemnitz, E., Eds.; Elsevier: Amsterdam, Netherlands, 2016; pp. 81–120; ISBN: 978-0-444-63587-7.
27. Kockmann, N. *Transport phenomena in micro process engineering*; Springer: New York City, NY, USA, 2008; ISBN 978-3-540-74616-4.
28. Matlosz, M.; Falk, L.; Commenge, J.-M. Process intensification. In *Microchemical engineering in practice*; Dietrich, T.R., Ed.; Wiley & Sons, Inc: Hoboken, NJ, USA, 2009; pp. 325–348; ISBN 978-0-470-23956-8.
29. Cybulski, A.; Moulijn J.A. *Structured Catalysts and Reactors*, 2nd ed.; CRC Press, Taylor & Francis Group: Boca Raton, FL, USA, 2005; pp. 1–18; ISBN: 978-1-4200-2800-3.
30. Mbodji, M.; Commenge, J.-M.; Falk, L. Preliminary design and simulation of a microstructured reactor for production of synthesis gas by steam methane reforming. *Chem. Eng. Res. Des.* **2014**, *92*, 1728–1739.
31. Metkar, P.S.; Salazar, N.; Muncrief, R.; Balakotaiah, V.; Harold, M.P. Selective catalytic reduction of NO with NH_3 on iron zeolite monolithic catalysts: Steady-state and transient kinetics. *Appl. Catal. B: Environ.* **2011**, *104*, 110–126.
32. Bhatia, D.; McCabe, R.W.; Harold, M.P.; Balakotaiah, V. Experimental and kinetic study of NO oxidation on model Pt catalysts. *J. Catal.* **2009**, *266*, 106–119.
33. Liao, C.; Erickson, P.A. Characteristic time as a descriptive parameter in steam reformation hydrogen production processes. *Int. J. Hydrogen Energy* **2008**, *33*, 1652–1660.
34. Beguin, B.; Garbowski, E.; Primet, M. Stabilization of alumina by addition of lanthanum. *Appl. Catal.* **1991**, *75*, 119–132.
35. Wijaya, W.Y.; Kawasaki, S.; Watanabe, H.; Okazaki, K. Damköhler number as a descriptive parameter in methanol steam reforming and its integration with absorption heat pump system. *Appl. Energy* **2012**, *94*, 141–147.
36. Stutz, M.J.; Poulikakos, D. Optimum washcoat thickness of a monolith reactor for syngas production by partial oxidation of methane. *Chem. Eng. Sci.* **2008**, *63*, 1761–1770.
37. Arzamendi, G.; Uriz, I.; Navajas, A.; Diéguez, P.M.; Gandía, L.M.; Montes, M.; Centeno, M.A.; Odriozola, J.A. A CFD study on the effect of the characteristic dimension of catalytic wall microreactors. *AIChE J.* **2011**, *58*, 2785–2797.
38. Arzamendi, G.; Diéguez, P.M.; Montes, M.; Odriozola, J.A.; Sousa-Aguiar, E.F.; Gandía, L.M. Methane steam reforming in a microchannel reactor for GTL intensification: A computational fluid dynamics simulation study. *Chem. Eng. J.* **2009**, *154*, 168–173.
39. Boldrini, D.E.; Sánchez M., J.F.; Tonetto, G.M.; Damiani, D.E. Monolithic stirrer reactor: Performance in the partial hydrogenation of sunflower oil. *Ind. Eng. Chem. Res.* **2012**, *51*, 12222–12232.
40. Dekker, F.H.M.; Bliek, A.; Kapteijn, F.; Moulijn, J.A. Analysis of mass and heat transfer in transient experiments over heterogeneous catalysts. *Chem. Eng. Sci.* **1995**, *50*, 3573–3580.
41. González-Castaño, M.; Ivanova, S.; Laguna, O.H.; Martínez T., L.M.; Centeno, M.A.; Odriozola, J.A. Structuring Pt/CeO_2/Al_2O_3 WGS catalyst: Introduction of buffer layer. *Appl. Catal. B Environ.* **2017**, *200*, 420–427.
42. Deutschmann, O.; Schwiedemoch, R.; Maier, L.I.; Chatterjee, D. Natural gas conversion in monolithic catalysts: Interaction of chemical reactions and transport phenomena. *Studies in Surface Science and Catalysis* **2001**, 251–258.